Microstructural Evolution and Bonding Behavior during Transient Liquid-Phase Bonding of a Duplex Stainless Steel using two Different Ni-B-Based Filler Materials

XINJIAN YUAN, MYUNG BOK KIM, and CHUNG YUN KANG

Microstructural evolution and bonding behavior of transient liquid-phase (TLP) bonded joint for a duplex stainless steel using MBF-30 (Ni-4.5Si-3.2B [wt pct]) and MBF-50 (Ni-7.5Si-1.4B-18.5Cr [wt pct]) were investigated. Using MBF-30, the microstructure of the athermally solidified zone was dependent on B diffusion at 1333.15 K (1060 °C). Ni_3B and a supersaturated γ-Ni phase were observed in this zone. BN appeared in the bonding-affected zone. However, using MBF-50, the influences of base metal alloying elements, particularly N and Cr as well as Si in the filler material, on the bond microstructure development were more pronounced at 1448.15 K (1175 °C). BN and $(Cr, Ni)_3Si$ phase were present in the bond centerline. The formation of BN precipitates in the bonding-affected zone was suppressed. A significant deviation in the isothermal solidification rate from the conventional TLP bonding diffusion models was observed in the joints prepared at 1448.15 K (1175 °C) using MBF-50.

I. INTRODUCTION

TRANSIENT liquid-phase (TLP) bonding has been considered an attractive alternate joining process for duplex stainless steels (DSSs).[1–5] The TLP bonding developed by Duvall et al.[6] is a hybrid joining process, which combines the beneficial features of liquid phase joining and diffusion bonding techniques.[7] In the TLP bonding process, an insert alloy containing melting point depressant elements is sandwiched between the base alloy surfaces, and then the assembly is heated to a temperature between the liquidus of the insert metal and that of the base metal. Generally, it is considered that four distinct stages are present during the TLP bonding process, namely dissolution of base metal, widening of interlayer, isothermal solidification of liquid, and homogenization of bond region. If sufficient time for complete isothermal solidification is not allowed at the bonding temperature, then the formation of eutectic microconstituents could occur along the bond centerline. It is normally the goal of the TLP bonding process to prevent the formation of these microconstituents as they have been deleterious to the mechanical properties of bonded metals.[8,9] Therefore, to achieve reliable TLP bonded joints, isothermal solidification has been recognized as the most important stage and the time required for isothermal solidification completion is a fundamentally important parameter during the TLP bonding. Several models of TLP bonding, most of which are based on binary phase relationships between the base and filler alloy, have been proposed to explain the microstructural development and model the isothermal solidification process.[10–13] Recently, Sinclair et al.[14] studied numerical modeling of isothermal solidification process in ternary systems and reported that the actual phase relationships encountered during TLP bonding of their multicomponent systems could cause a significant modification of isothermal solidification behavior in contrast to conventional expectations. Littke work has been done regarding this discrepancy in duplex stainless steel. Therefore, the objective of the present research is to investigate and interpret the notable variations sufficiently in the microstructure evolution and bonding behavior during TLP bonding of a DSS using two different Ni-B-based filler metals.

II. EXPERIMENTAL PROCEDURE

A nitrogen-containing DSS and four Ni-B-based amorphous foils with a thickness of 25.4 μm, MBF-30, MBF-50, MBF-80, and MBF-35 (Hitachi Metals Ltd., Tokyo, Japan), were used as the base alloy and the filler metals, respectively. The use of MBF-80 and MBF-35 was to clarify and explain the effects of Cr and Si on joint microstructure and isothermal solidification. The chemical compositions and the melting ranges of these materials are shown in Table I. The $10 \times 10 \times 10$ mm^3 specimens were cut from the as-received DSS plates (10-mm thick). Thereafter, the faying surfaces of the specimens were ground with 120- to 1500-grade SiC papers and ultrasonically cleaned in a solution of acetone for 60 minutes prior to the TLP bonding. Subsequent to this, the filler material was placed between the mating surfaces of the cleaned specimens, shown schematically in Figure 1. In addition, a stainless

XINJIAN YUAN, Doctoral Candidate, MYUNG BOK KIM, Graduate Student, and CHUNG YUN KANG, Professor, are with the Department of Materials Science and Engineering, Pusan National University, Busan 609735, Republic of Korea. Contact e-mail: kangcy@pusan.ac.kr

Table I. Chemical Composition of Materials Employed and the Melting Ranges of the Filler Materials Determined by a Differential Scanning Calorimetry

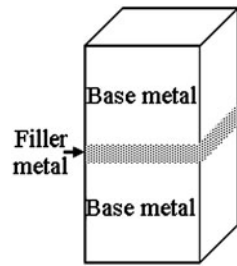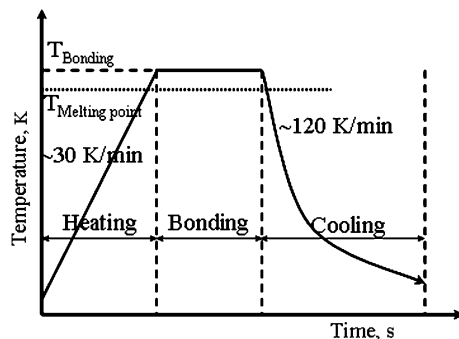| Materials	Nominal Composition (Weight Percent)												Melting Range K (°C)
	Fe	N	C	Si	Mn	P	S	Cu	Ni	Cr	Mo	B	
DSS	Bal.	0.16	0.03	0.39	1.41	0.02	0.003	0.19	5.86	22.40	3.49	—	—
MBF-30	—	—	—	4.5	—	—	—	—	Bal.	—	—	3.2	1253.15 to 1313.15 (980 to 1040)
MBF-50	—	—	—	7.5	—	—	—	—	Bal.	18.5	—	1.4	1338.15 to 1423.15 (1065 to 1150)
MBF-80	—	—	—	—	—	—	—	—	Bal.	15.2	—	4.0	1293.15 to 1338.15 (1020 to 1065)
MBF-35	—	—	—	7.3	—	—	—	—	Bal.	—	—	2.2	1233.15 to 1283.15 (960 to 1010)

Fig. 1—Schematic of bonding setup.

Fig. 2—Schematic of the TLP bonding cycle.

steel fixture was used to fix the specimens and to hold the sandwich assembly during the bonding operation. The TLP bonding operation was carried out in a vacuum furnace, operating under a vacuum of approximately 10^{-4} Torr, using a temperature-time bonding cycle shown schematically in Figure 2. The heating rate between room and bonding temperature was ~30 K/min. After joining, the specimens were cooled in the vacuum furnace by switching off the furnace; the cooling rate was around ~120 K/min. The bonding schedule is given in Table II.

After bonding, specimens for metallographic examination were sectioned from the TLP-bonded joints. Ground and polished specimens were etched electrolytically at 3 V in an etchant containing 5 ml of H_2SO_4 and 95 ml of distilled water for the joints prepared using MBF-30 and another etchant consisting of 5 g of $H_2C_2O_4$ and 100 ml of distilled water for the joints made using MBF-50 and MBF-80. Microstructural observations were conducted using an optical microscope and a Hitachi S-4700 field emission scanning electron microscope (FE-SEM, Japan Electron Optics Ltd., Tokyo, Japan). The chemical composition was analyzed using a JEOL JXA-8100 electron probe X-ray microanalyzer (EMPA, Japan Electron Optics Ltd., Tokyo, Japan) supplemented to spot and line scan wavelength dispersive spectrometry. An average of three measurements was carried out for each phase. The presence of light elements like B and N also was detected by a MICROLAB 350 Auger electron spectroscopy (AES). Phase compositions in the bonded joints were identified using X-ray diffraction (XRD) (with CuK_α radiation).

III. RESULTS AND DISCUSSION

Figure 3 shows typical cross-sectional SEM images of the joint for DSS using MBF-30 prepared at 1333.15 K (1060 °C) for 60 seconds. Figure 3 shows that the joint region consisted of the following distinct microstructural zones, prior to completion of isothermal solidification:[3]

(a) Isothermally solidified zone (ISZ), which consisted of a proeutectic γ-Ni solid solution phase. Some Ni_3Si precipitates with granular morphology were present in the ISZ adjacent to the remaining melt as shown in Figure 3(b). A compositional shift resulted from interdiffusion of alloying elements between the interlayer and the substrate during holding at a constant temperature, which is the driving force for isothermal solidification.

(b) Athermally solidified zone (ASZ), which consisted of a supersaturated γ-Ni rich in B and Ni_3B with a regular pattern. The formation of this zone is a result of insufficient time for isothermal solidification completion. Cooling is the main driving force for athermal solidification.

(c) Bonding-affected zone (BAZ contained BN particles with blocky morphology owing to B diffusion into the interlayer–substrate interface and the adjacent base metal during the TLP bonding.

Figure 4(a) represents optical microstructure of the joint for DSS using MBF-30 prepared at 1333.15 K (1060 °C) for 300 seconds. It can be observed that the joint was free from the remaining melt. Thus, isothermal solidification of the liquid in the joint centerline was completed within 300 seconds at 1333.15 K (1060 °C).

Table II. TLP Bonding Tests Matrix

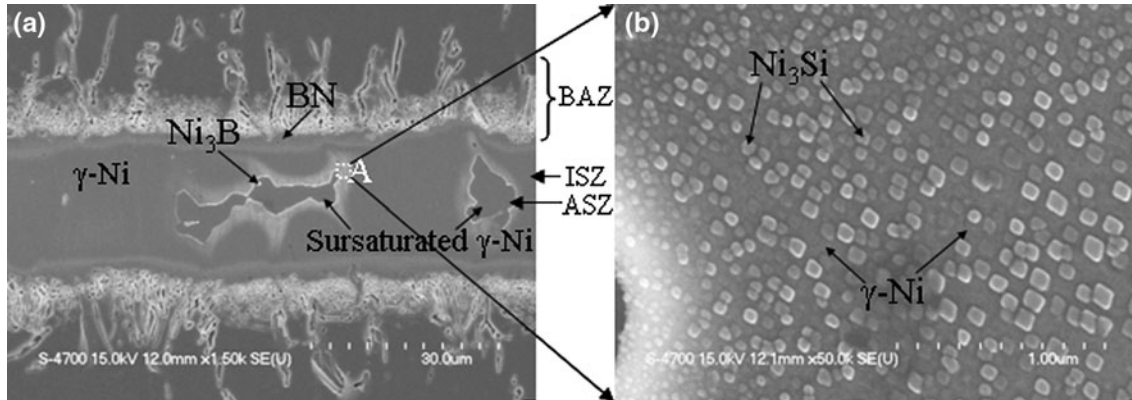| Filler Metal	Bonding Temperature K (°C)	Bonding Time (s)										
MBF-30	1333.15 (1060)	60	120	300	—	—	—	—	—	—	—	—
	1343.15 (1070)	—	—	300	—	—	—	—	—	—	—	—
	1428.15 (1155)	—	—	300	—	—	—	—	—	—	—	—
	1448.15 (1175)	—	—	300	—	—	—	—	—	—	—	—
MBF-50	1428.15 (1155)	—	—	—	—	1800	—	—	—	—	—	—
	1448.15 (1175)	—	—	300	900	1800	2700	3600	5400	7200	10,800	14,400
MBF-80	1343.15 (1070)	—	—	300	—	—	—	—	—	—	—	—
MBF-35	1333.15 (1060)	—	—	300	—	—	—	—	—	—	—	—

Fig. 3—Typical microstructure of the bond prepared using MBF-30 at 1333.15 K (1060 °C) after 60 s: (*a*) overview, (*b*) magnified morphology in zone "A."
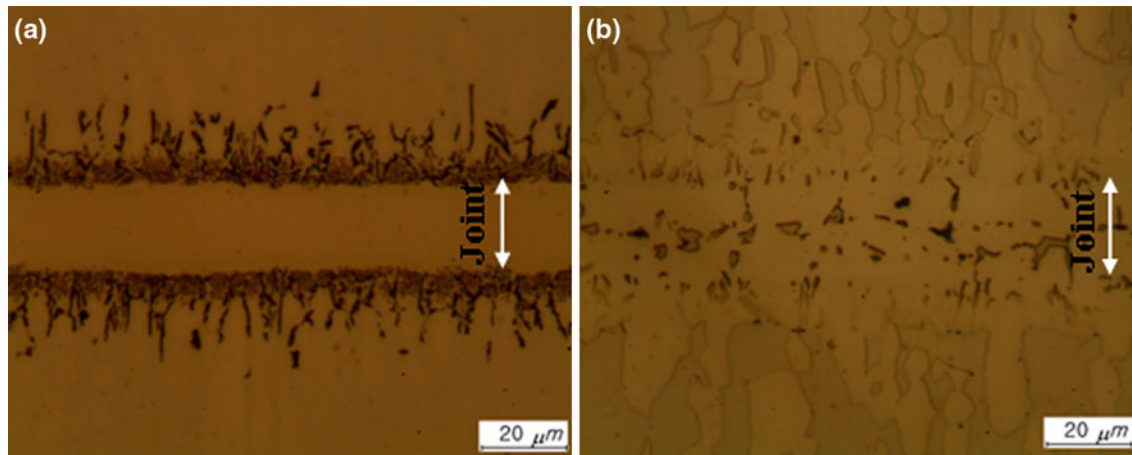

Fig. 4—Typical microstructure of the bonds prepared for 300 s at (*a*) 1333.15 K (1060 °C) using MBF-30 and (*b*) at 1448.15 K (1175 °C) using MBF-50.

Figure 4(a) also shows no Ni-silicide was found in the bonded interlayer.

However, Figure 4(b) illustrates an optical microstructure of the joint for DSS using MBF-50 made at 1448.15 K (1175 °C) for 300 seconds showing the residual liquid. The details of the joint centerline microstructure are delineated in Figure 5. Table III illustrates the chemical compositions analyzed by EPMA of the zone shown in Figure 5(b). Figures 6 and 7 present X-ray line scans taken across the phases in joint centerline. The results suggest the ASZ microstructure consisted of BN and a silicide named as $(Cr, Ni)_3Si$ incorporating N, and the microstructure of the ISZ consisted of γ-Ni phase. The appearance of B and N in black particles (Figure 5) was verified by the AES results shown in Figure 8. Some C and O peaks also were observed in Figure 8, although specimens were sputtered with 3 keV Ar^+ ions for 10 minutes prior to the Auger electron spectroscopic measurement to remove the surface contamination. C and O were the
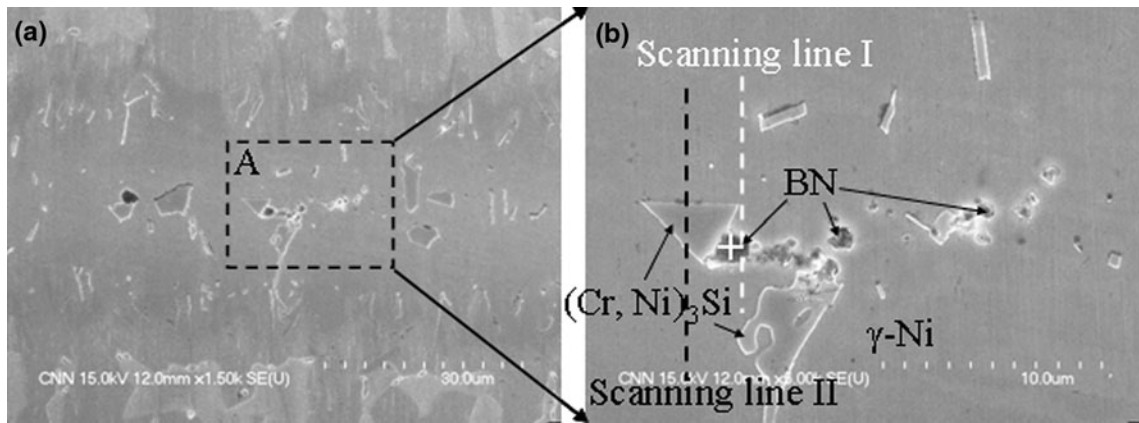
Fig. 5—SEM images of the bond prepared using MBF-50 at 1448.15 K (1175 °C) after 300 s: (*a*) overview, (*b*) magnified morphology in zone "A."

Table III. EPMA Compositional Analyses of Different Phases Present in the Bond Region Made using MBF-50 at 1448.15 K (1175 °C) for 300 Seconds

Elements (At. Pct)	BN	$(Cr, Ni)_3Si$	Proeutectic γ-Ni
B	33.69	—	—
Ni	18.95	27.75	50.05
Cr	11.11	38.84	21.46
Si	2.87	14.94	10.21
N	22.87	13.95	—
Fe	10.34	1.99	17.88
Mo	0.17	2.53	0.40

dominating contaminants in the specimens. However, if no sputtering treatment took place, then Auger peaks of C and O were markedly high. To study the microstructure of the bonded interlayer from another direction, the joint obtained using MBF-50 at 1448.15 K (1175 °C) for 300 seconds was ground and polished along a direction parallel to the interlayer–substrate interface. SEM images and XRD patterns then were recorded, the results of which are shown in Figures 9 and 10. Figure 10 confirms the existence of BN and $(Cr, Ni)_3Si$ in bonded interlayer. Therefore, it could be concluded that the resultant microstructure of the remaining melt contained BN and $(Cr, Ni)_3Si$ rich in N.

It is interesting to note that the bonds for DSS using MBF-50 produced at 1448.15 K (1175 °C) for varying times ranging between 60 and 14400 seconds were free of secondary-phase precipitates, BN, in the BAZ (*e.g.*, Figure 4(b)). In addition, Ni_3B was not detected in the bonded interlayer. However, some BN precipitates were observed in the bonded interlayer (Figure 5(b)).

To investigate the effect of bonding temperature on the microstructure evolution, DSS|MBF-30 and DSS|MBF-50 specimens were performed at 1428.15 K and 1448.15 K (1155 °C and 1175 °C) for 300 seconds and for 1800 seconds, respectively. Figure 11 illustrates SEM images of joints prepared using MBF-30 at 1428.15 K and 1448.15 K (1155 °C and 1175 °C) for 300 seconds, and Figure 12 shows an X-ray line scan taken across the secondary phase in the bonded
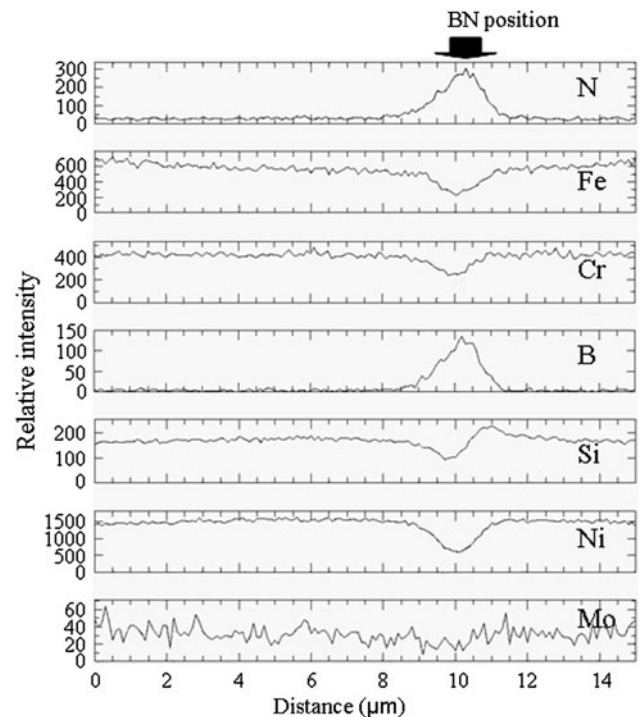

Fig. 6—Electron microprobe analysis (X-ray line scan) of black particle in the centerline region of the bond made using MBF-50 at 1448.15 K (1175 °C) for 300 s, with the white dot line I in Fig. 5(b) showing the line scan trace.

interlayer. Clearly, BN precipitates were detected in the joint centerline. Furthermore, the size of BN enlarged as the bonding temperature increased. Figure 13 shows optical and SEM images of joints made using MBF-50 at 1428.15 K and 1448.15 K (1155 °C and 1175 °C) for 1800 seconds, and Figure 14 indicates an X-ray line scan taken across a precipitate. No BN precipitates were observed in the interface of the joints. Figure 13 obviously indicated that, at 1428.15 K (1155 °C), BN secondary phases appeared in the position adjacent to the bond centerline, whereas at 1448.15 K (1175 °C), BN precipitates were present along the centerline region.
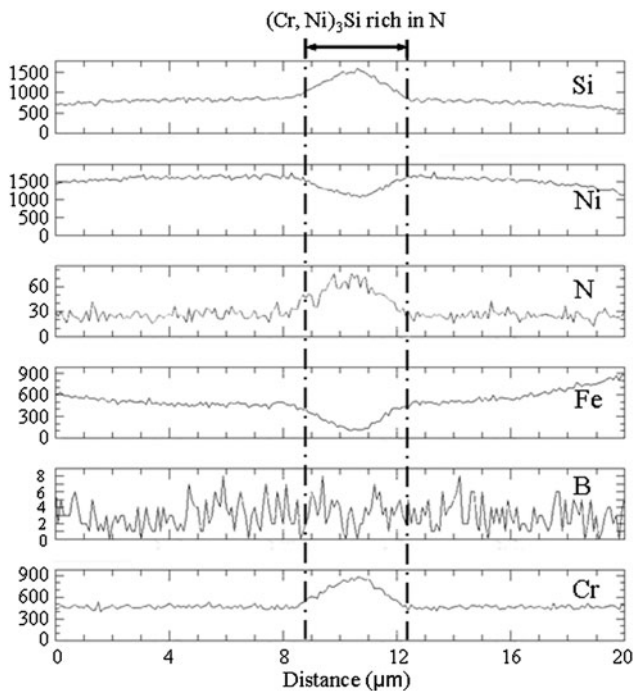
Fig. 7—Electron microprobe analysis (X-ray line scan) of angular phase in the centerline region of the bond made using MBF-50 at 1448.15 K (1175 °C) for 300 s, with the black dot line II in Fig. 5(b) showing the line scan trace.

To understand the effect of Si on the joint microstructure, MBF-30 and MBF-35 were used as the filler metals and bonding operations were conducted at the same temperature—1333.15 K (1060 °C), for 300 seconds because MBF-35 is similar in Si concentration to MBF-50 and does not have any Cr content. Using MBF-30, the microstructure of the joint and the extent of isothermal solidification were controlled by the influence of B. In MBF-35, the residual liquid also was observed in the joint centerline after 300 seconds, and the microstructure of the ASZ mainly contained Ni3Si. The time required to eliminate the remaining melt was within 2700 seconds, which was long compared with MBF-30, although MBF-35 has a relatively low B content. The detailed results are not shown in this study because they are reported in detail in previous work.[5] Thus, Si in MBF-50 has an influence on bond microstructure and isothermal solidification.

To interpret the influence of Cr on the microstructure of the joint region, DSS|MBF-30 and DSS|MBF-80 systems were carried out for 300 seconds at 1343.15 K (1070 °C) because the melting range of MBF-80 is 1293.15 K to 1338 K (1020 °C to 1065 °C). The joint obtained using MBF-30 at 1343.15 K (1070 °C) for 300 seconds (Figure 15) was similar to that in Figure 4(a), which was free from the residual liquid. From backscatter electron images (Figure 16) of the joint obtained using MBF-80 at 1343.15 K (1070 °C) for 300 seconds, however, the isothermal solidification of the liquid MBF-80 was not completed, and the joint centerline contained the eutectic constituents of Ni3B, Cr-borides, and γ-Ni, which are characteristic of those observed.[4]

Based on these results, Figure 17 shows the schematic model of the microstructural evolution of the joint region as functions of Cr and Si contents and bonding temperature. The DSS bonded using MBF-30 at lower temperatures, 1333.15 K and 1343.15 K (1060 °C and 1070 °C), is free from the residual liquid in the bond centerline. With increasing Cr content in the insert alloy, the microstructure of the athermally solidified zone in the joint obtained using MBF-80 contains γ-Ni, Ni3B, and Cr-borides. By increasing the Si content in the filler, Ni3Si remained in the joint centerline. The bonded interlayer conducted with MBF-30 at higher temperatures, 1428.15 K and 1448.15 K (1155 °C and 1175 °C), consists of BN and γ-Ni; when using MBF-50 at temperatures varying from 1428.15 K to 1448.15 (1155 °C to 1175 °C,) the position of formation for BN in the bonded interlayer moves toward the centerline region. Additionally, the interface was free of BN when using the insert alloy (MBF-50) and conducted at higher temperatures, 1428.15 K and 1448.15 K (1155 °C and 1175 °C), whereas BN appears at the interface for MBF-30, MBF-80, and MBF-35. Thus, the formation mechanism of microstructural changes in the interface and the bond centerline might be explained in Sections III–A, III–B, and III–C.

A. BN Precipitates in the Bonding-Affected Zone Using MBF-30 at 1333.15 K (1060 °C)

The formation of BN in the BAZ during TLP bonding of DSS using MBF-30 at 1333.15 K (1060 °C) can be interpreted based on the following two mechanisms:

First, the conventional TLP models assume sequential liquid–solid equilibration and solid diffusion of melting point depressant element (B). Hence, the interlayer alloy upon melting rapidly attains equilibrium with the solid base metal, which involves the base metal dissolution, after which, the solid-state diffusion of B commences. Under these conditions, no boride precipitation is expected during the TLP bonding process because it is considered that the solute diffusion in the base metal occurs under equilibrium conditions subsequent to the liquid–solid equilibration involving the base metal dissolution.[15] It is suggested that, contrary to the predictions of currently conventional TLP models, a notable solid-state diffusion of B from the liquid into the solid substrate takes place prior to the completion of the dissolution process,[16,17] which can cause the development of significant B concentration in the substrate. As evidenced by a recent study, Kuntz et al. have suggested that the loss of the initial liquid formed during short isothermal hold times could be caused by a transient influence at the beginning of the isothermal process.[18] When the B concentration in the BAZ exceeds the solubility limit of B at the bonding temperature, the precipitation of secondary phases in this region is expected.

Second, Pouranvari et al.[19] have proposed that it is based on the diffusion of B into the solid substrate during the isothermal solidification stage. The isothermal solidification process is controlled by B diffusion out of the liquid into the solid substrate. In the BAZ, this diffusion
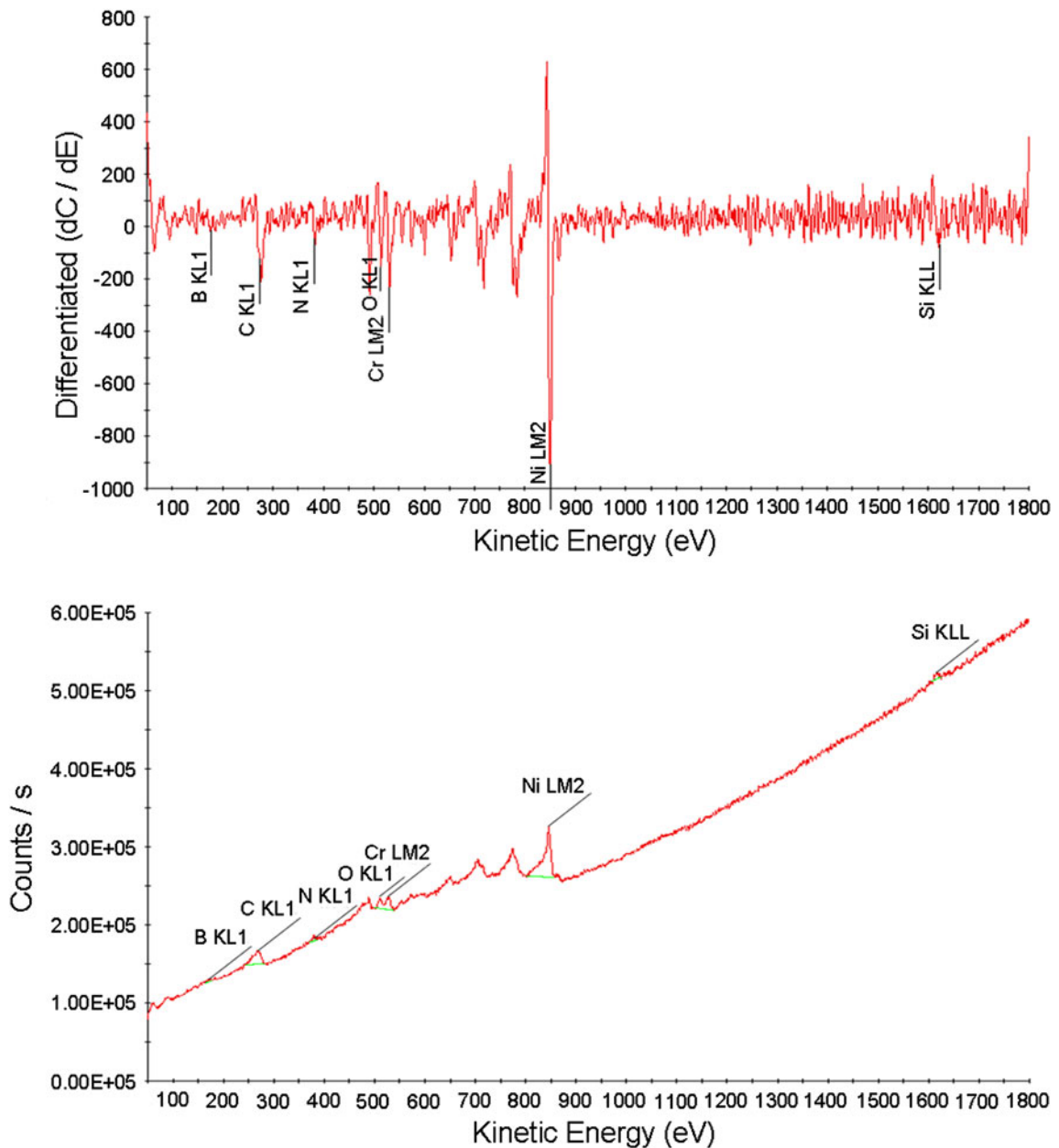
Fig. 8—Auger electron spectra of black particle in the centerline region of the bond made using MBF-50 at 1448.15 K (1175 °C) for 300 s, with the "+"in Fig. 5(b) showing the detecting region.

of B and the appearance of N, which is a strong boride-forming element, can explain the formation of BN. That is because BN is more stable than those of other borides.[3,4,20] According to this mechanism, B and N concentration profiles across the joint and the resulting microstructure can be illustrated schematically as shown in Figure 18(a). The ejection of B into adjacent melt because of low solubility of B in Ni (0.3 at. pct[15,21–27] presented in Table IV) and the partition coefficient of B in Ni (~0.008, based on the Ni-B binary phase diagram[22,27]) shifts the melt composition toward the eutectic composition. The enrichment of B and the formation of Ni$_3$B lead to an increase in B concentration in the ASZ. The B concentration in the ISZ is above the B solubility limit in the base metal. The local increase in

B content in the BAZ is caused by BN precipitation in this region. Correspondingly, an increase in N concentration in the BAZ is also caused by the formation of BN in this zone. The amount of B, which can diffuse through the ISZ into the substrate, is dependent on B solubility at the liquid–ISZ interface ($C_{\alpha L}$).

B. No BN Precipitates in the Bonding-Affected Zone Using MBF-50 at 1448.15 K (1175 °C)

No BN was observed in the BAZ, although the bonding temperature of 1448.15 K (1175 °C) when using MBF-50 is still lower than the BN solidus temperature. This might be explained in the following paragraphs.
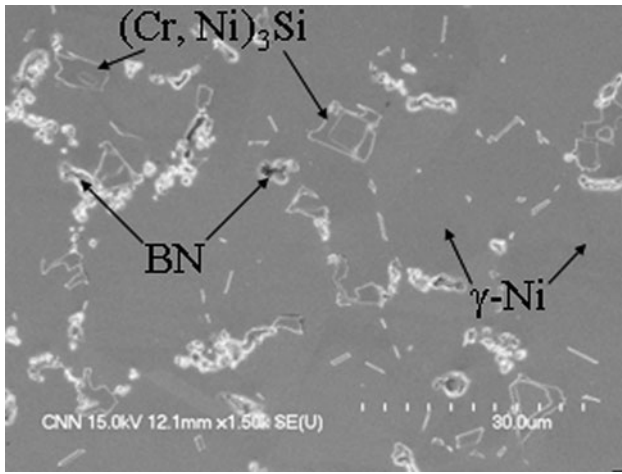
Fig. 9—Typical SEM image examined after polishing along a direction parallel to the interlayer–substrate interface and observing centerline region of the bond made using MBF-50 at 1448.15 K (1175 °C) for 300 s.
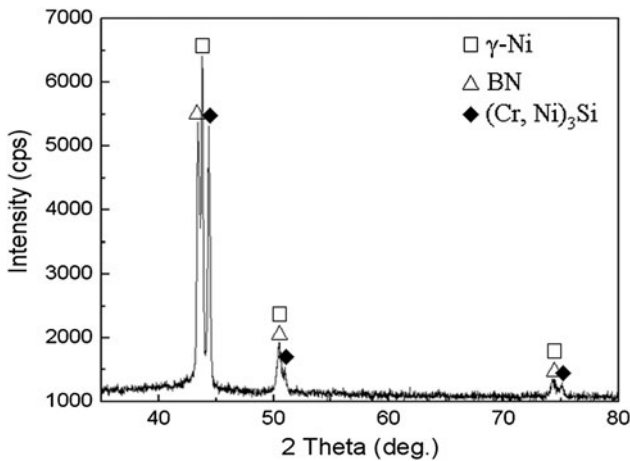

Fig. 10—XRD patterns examined after polishing along a direction parallel to the interlayer–substrate interface and analyzing centerline region of the bond made using MBF-50 at 1448.15 K (1175 °C) for 300 s.
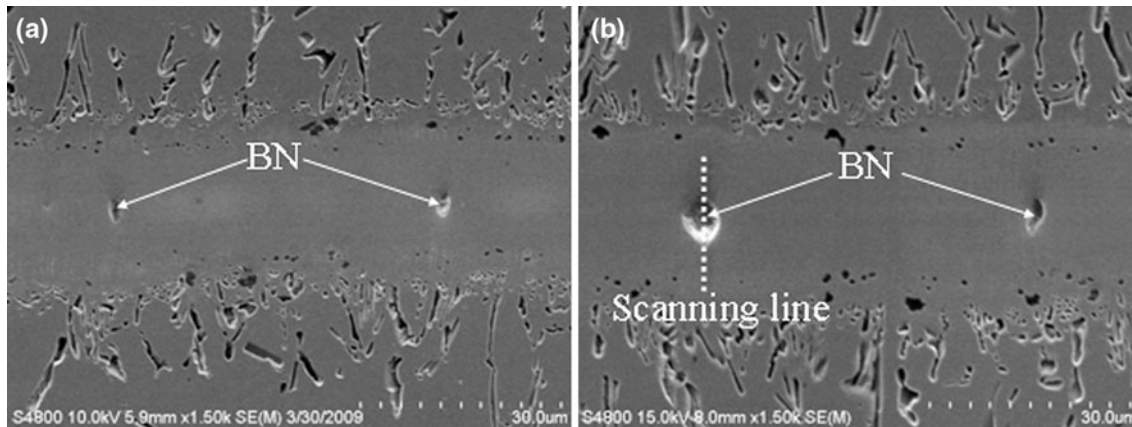
First, based on a derivation of the Nernst–Brunner theory, the dissolution stage has already been modeled as follows[31,32]:

$$C = C_{\text{sat}} \left[1 - \exp\left(\frac{KAt}{V}\right) \right] \qquad [1]$$

where C is the solute (B) concentration in the liquid at time t; C_{sat} is the saturated solute concentration in the liquid at equilibrium; K is the dissolution rate constant; A is the area of the solid–liquid interface; V is the volume of the liquid phase ($A/V = 1/w$, where w is the gap width); t is the holding time. K increases sharply with an increasing bonding temperature based on the temperature-dependent Arrhenius-type equation.[32] Nishimoto et al.[32] reported that K is 0.09, 0.80, and 6.75 at 1373.15 K, 1453.15 K, and 1523.15 K (1100 °C, 1180 °C, and 1250 °C), respectively, during TLP bonding of CMSX-2 Ni-based single crystal superalloy using a Ni-Cr-B insert alloy. According to Eq. [1], the time required for the base metal dissolution to be completed decreases obviously with an increase in K. Consequently, the decreased time available for the diffusion of B during the base metal dissolution stage might result in the suppression of BN formation in the BAZ.

Second, from Table IV, the solubility limit of B in Fe, taken to be 0.1 at. pct,[25,28–30] is one third of that in Ni (0.3 at. pct).[15,21–27] Thus, at the higher bonding temperature used in the present work, on the one hand, the solubility of the melting point depressant B in the ISZ is decreased (i.e., $C_{\alpha L}$ is decreased), as shown in Figure 18(b), owing to more diffusion of the base alloying elements, particularly Fe, from the substrate into the interlayer. In addition, according to the Ni-B phase diagram, an increase in bonding temperature above the eutectic temperature simultaneously reduces the solubility of B in Ni.[22] A decrease in the solubility of B in Ni from 320 ppm at 1398.15 K (1125 °C) to 210 ppm at 1498.15 K (1225 °C) has been reported by Ramirez and Liu.[33] B solubility in Ni ($C_{L\alpha}$) is decreased. On the other hand, more diffusion of Ni from the interlayer into the substrate leads to an increase in maximum solubility of B in the base metal (C_S^M) (Figure 18(b)). Thus, the decrease in $C_{\alpha L}$ and the

Fig. 11—SEM images of the bonds prepared with MBF-30 for 300 s at (a) 1428.15 K (1155 °C) and (b) 1448.15 K (1175 °C).
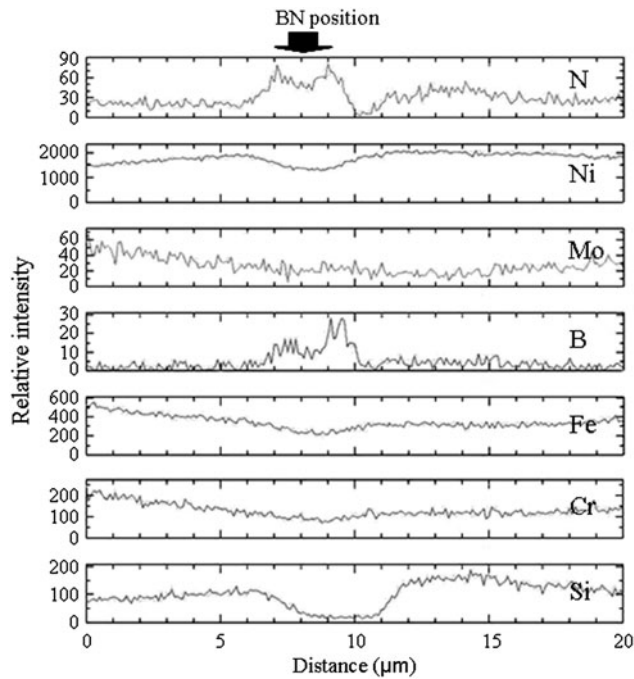
Fig. 12—Typical electron microprobe analysis (X-ray line scan) of secondary phase in the centerline region of the joint prepared with MBF-30 at 1448.15 K (1175 °C) for 300 s. The white dot line in Fig. 11(b) indicates the line scan path.

increase in C_S^M with an increase in bonding temperature could be contributed to a decrease in the concentration gradient with distance between the ISZ and the substrate. Therefore, this may cause a reduction in the driving force for the diffusion of B and thus the suppression of BN precipitation in the BAZ.

Third, using MBF-50, a considerable enrichment of the liquated insert with Cr is caused by a substantial Cr element (18.5 wt pct Cr) contained in this insert alloy. As mentioned previously, conducted at 1343.15 K (1070 °C) using MBF-80, the increased Cr in the filler metal produced the joint with ternary eutectic phases along the centerline region after holding for the same time in contrast to MBF-30. This indicates that the third element, Cr, might hinder the migration of B from the interlayer into the substrate. Thus, the suppression of BN in the BAZ could be generated.

Finally, the diffusion of N from the base metal into the interlayer is accelerated significantly when the bonding temperature is increased. BN is formed in the bonded interlayer during cooling. As mentioned earlier, using MBF-30 at 1428.15 K and 1448.15 K (1155 °C and 1175 °C) (Figure 11), the increase in the size of BN as a function of temperature demonstrates that more diffusion of N occurs out of the substrate into the interlayer with an increase in bonding temperature. Additionally, B impoverishment in the BAZ results from
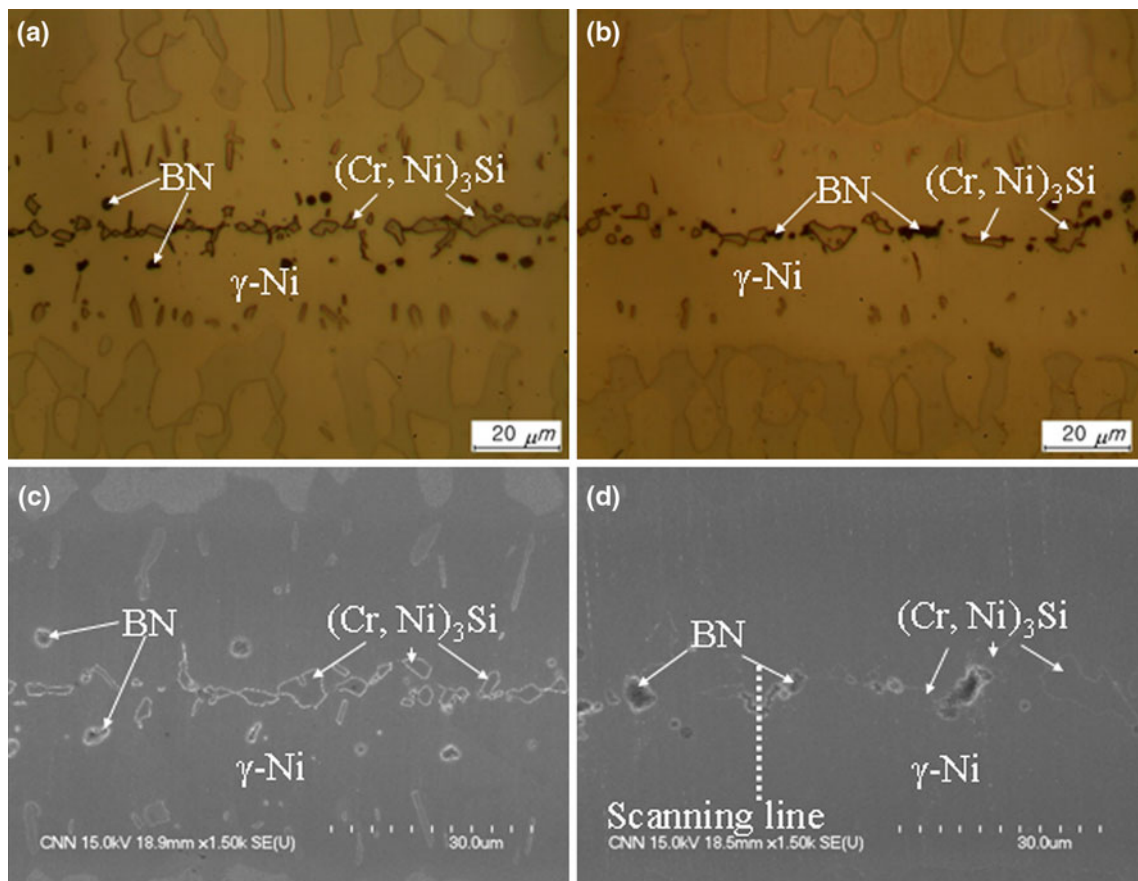

Fig. 13—Optical and SEM images of the bonds made with MBF-50 for 1800 s at 1428.15 K (1155 °C) (*a* and *c*) and 1448.15 K (1175 °C) (*b* and *d*).
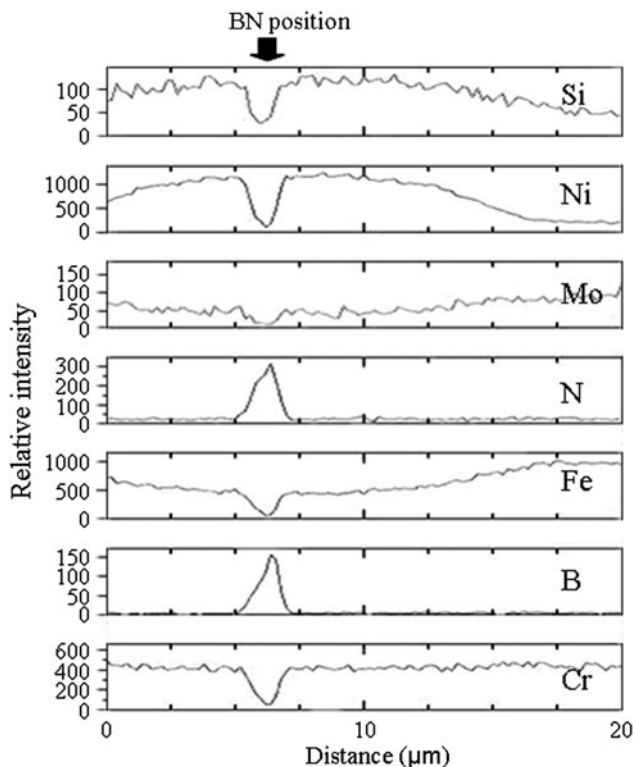
Fig. 14—Typical electron microprobe analysis (X-ray line scan) of secondary phase in the centerline region of the joint made at 1448.15 K (1175 °C) for 1800 s using MBF-50. The white dot line in Fig. 13(d) indicates the line scan path.
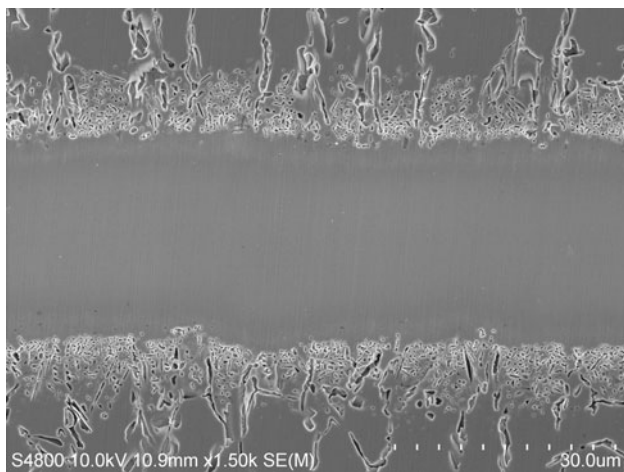

Fig. 15—Typical SEM image of the joint prepared using MBF-30 at 1343.15 K (1070 °C) for 300 s.

B diffusion suppressed by these three factors when conducted at 1448.15 K (1175 °C) using MBF-50. A lack of this driving source in this zone forces N diffusion to change its destination from the interface to the interlayer. Thus, N concentration in the BAZ at 1448.15 K (1175 °C) using MBF-50 is smaller than that at 1333.15 K (1060 °C) using MBF-30. Therefore, the destination of N diffusion changed from the interface to the interlayer, and more diffusion of N into the

interlayer might be responsible for the suppression of BN formation in the BAZ at 1448.15 K (1175 °C).

Therefore, considering these four factors, it seems that a joint interface free from BN precipitates can be expected. Similarly, a reduction in the volume fraction of borides at a high bonding temperature during TLP bonding of a CMSX-4 Ni-based single crystal superalloy using a Ni-Cr-Co-Al-Ta-B insert alloy has been reported by Schnell[34] and Schnell and Graf.[35] They suggest that the B solubility in the isothermally solidified layer is reduced to the solubility of the parent metal above a critical temperature.

C. Change in Phase at the Bond Centerline

The ASZ microstructure in the bonds made at 1333.15 K (1060 °C) using MBF-30 depends on the segregation of melting point depressant elements during nonequilibrium solidification. As discussed, the ejection of B into the adjacent melt owing to low solubility of B in Ni[15,21–27] as well as the partition coefficient of B in Ni[22,27] shifts the liquid composition toward the eutectic composition. Consequently, the B-enriched γ-Ni and Ni_3B form as solidification progresses. A low solubility and low partition of B in Ni lead to the formation of this intermetallic phase. In addition, the enrichment of B and the relative impoverishment of Si were detected in the ASZ, after holding for 60 seconds.[3] Thus, it could be considered that the bond microstructure and the rate of isothermal solidification at a lower temperature is controlled by the diffusion of B.

Based on the microstructural study of the specimen bonded with MBF-50 at 1448.15 K (1175 °C), the microstructure of the joint centerline is governed by the segregation of the base metal alloying elements, particularly N, and the notable presence of Cr and Si. More dissolution of base metal alloying elements and more diffusion of N into the interlayer during the isothermal solidification process at 1448.15 K (1175 °C) in contrast to a lower bonding temperature control the microstructural development in the bond centerline. Although N in the base metal has only 0.16 wt pct, the substrate could provide the interface region and the bonded interlayer with sufficient N. On the one hand, the width of the base alloy is markedly larger in contrast to the insert alloy. Thus, the base material provides an infinite source of N. On the other hand, the residual liquid at the bonding temperature could have much more N content and be considered a driving force for the migration of N. Thus, the enrichment of N in the residual liquid could be generated. What is more, an increase in Si concentration in the filler material and low diffusivity of Si in Ni as compared with B could enhance a possibility in the presence of silicide in the bonded interlayer. Therefore, as mentioned previously, considering B diffusion suppressed by three factors (the decreased time available for diffusion of B during base metal dissolution stage, the reduction in concentration gradient of B between the interlayer and the substrate, and the notable enrichment of the liquated insert with Cr) as well as more diffusion of N into the interlayer at the elevated temperature, the formation of BN and
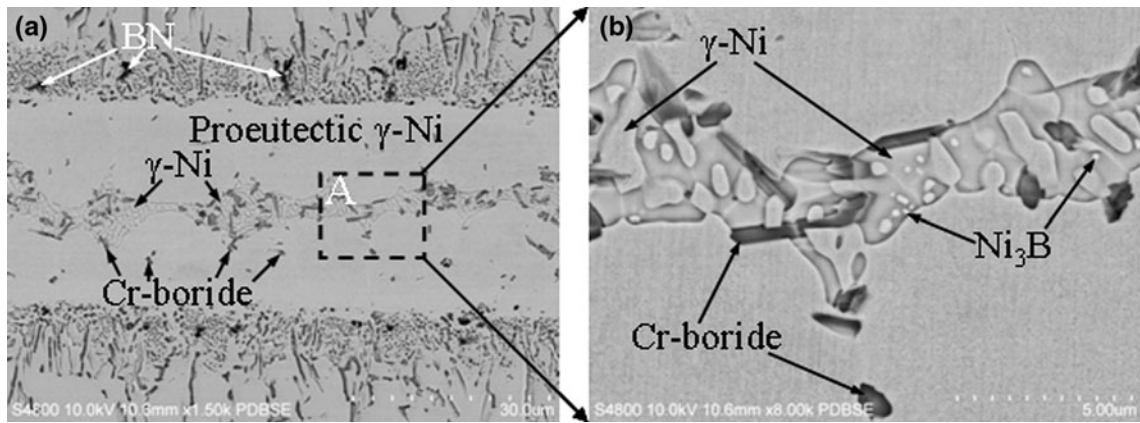
Fig. 16—Typical backscatter electron images of the joint obtained using MBF-80 at 1343.15 K (1070 °C) for 300 s: (a) overview, (b) magnified morphology in zone "A.".
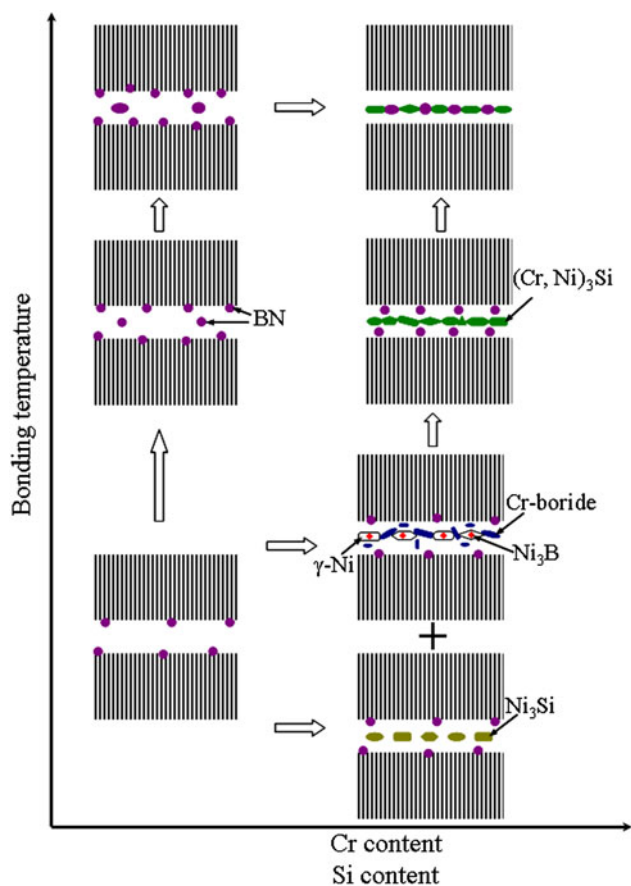

Fig. 17—Schematic model of the microstructural evolution in the joint region as functions of bonding temperature, Cr and Si.

N-rich (Cr, Ni)$_3$Si in the centerline region can be explained.

D. Comparison of Complete Isothermal Solidification Time in a Conventional Model and the Experiment

In conventional TLP bonding, because isothermal solidification of the liquid at a constant bonding temperature is dominated by solid-state diffusion of melting point depressant element,[26] the bonding temperature has a strong influence on the isothermal solidification. The increased temperature causes an increase in the diffusivity of the melting point depressant element. Sakamoto et al.[36] have proposed a linear relation between maximum clearance free from eutectic and a brazing parameter, $(T + 20 \log t)^{1/2}$, where T is the bonding temperature and t is the holding time. Therefore, it is suggested that the increasing bonding temperature results in a shorter complete isothermal solidification time (t_{IS}).

Several approaches have been proposed and developed to model the isothermal solidification process. Assuming that base metal dissolution and isothermal solidification stage could occur simultaneously instead of sequentially, the solute distribution approach is used by Gale and Wallach[16,23] for predicting t_{IS} based on the application of Fick's second law of diffusion by the following equation:[37]

$$C(x,t) = C_M + \frac{1}{2}(C_0 - C_M)\left\{ \operatorname{erf}\left(\frac{x+h}{\sqrt{4Dt}}\right) - \operatorname{erf}\left(\frac{x-h}{\sqrt{4Dt}}\right) \right\}$$

[2]

where D is the diffusion coefficient of the solute; $C(x, t)$ is the solute concentration as a function of distance from the center of the interlayer (x) and time (t); C_0 is the original solute concentration in the interlayer; C_M is the initial solute concentration in the substrate; and h is the initial half thickness of the inserted interlayer.

Isothermal solidification is considered to be complete when the concentration of the melting point depressant solute at the center of the remaining liquid is reduced to the value of concentration of this solute at the solidus, C_s. Thus, the solute concentration at the center of the interlayer is reduced to the solvus value, C_s, which is shown in the following equation:

$$C(x,t) = C_s, \quad x = 0$$

[3]

\ Substituting Eq. [3] into Eq. [2] yields the following:

$$\frac{C_s - C_M}{C_0 - C_M} = \operatorname{erf}\left(\frac{h}{\sqrt{4Dt_{IS}}}\right)$$
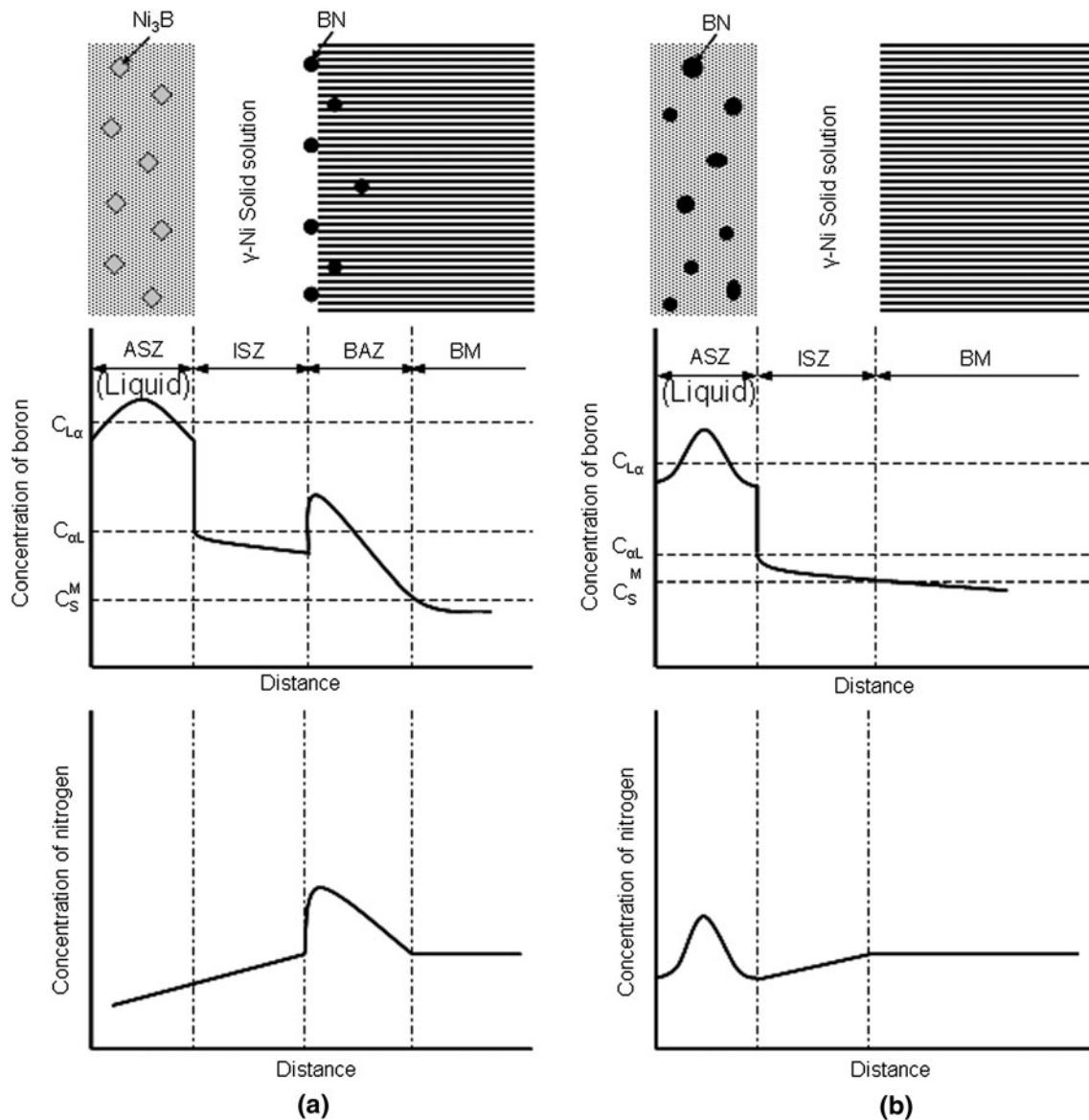
[4]

Fig. 18—B and N concentration profile and the resulting bond microstructure for bonding temperature of (a) 1333.15 K (1060 °C) using MBF-30 and (b) 1448.15 K (1175 °C) using MBF-50.

Gale and Wallach[16,23] have been reported a good agreement between estimated and experimental values of t_{IS} using this model. To apply this approach to the present study, C_M is taken to be 0 at. pct and C_s is regarded as 0.3 at. pct,[15,21–27] as shown in Table IV. The initial B concentrations in the interlayer, C_0, are 14.60 at. pct (3.2 wt pct) for MBF-30 and 6.53 at. pct (1.4 wt pct) for MBF-50, respectively. The diffusion coefficients subsequently are calculated by the following well-established Arrhenius equation:

$$D = D_0 \exp\left(\frac{-Q}{RT}\right) \qquad [5]$$

where Q is the apparent activation energy for boron diffusion, D_0 is the frequency factor, and R is the gas constant. The diffusion coefficients of B in Ni were evaluated using activation energy (Q = 211 kJ/mol[15]

and the vibration factor (D_0 = 1.44 × 10^{-2} m^2/s[15]). Thus, when lattice diffusion was mainly considered in the model, the calculated diffusivities of B solute in the Ni solvent, at 1333.15 K and 1448.15 K (1060 °C and 1175 °C), were 0.787 × 10^{-10} and 3.57 × 10^{-10} m^2/s, respectively.

For MBF-30, t_{IS} predicted in terms of this approach was 1420 seconds at 1333.15 K (1060 °C). When using MBF-50, this estimated value was only 71 seconds at 1448.15 K (1175 °C). The latter was markedly less than the former. The big difference in t_{IS} suggests that an increase in bonding temperature could produce an increased rate of isothermal solidification.

From Figure 4(a), the specimen bonded at 1333.15 K (1060 °C) for 300 seconds using MBF-30 was free from an eutectic microconstituent, which suggests the occurrence of a complete isothermal solidification. However, in MBF-50, conducted at 1448.15 K (1175 °C) for

300 seconds (Figure 4(b)), 1800 seconds (Figure 13(d)), 2700 seconds (Figure 19(a)), 3600 s (Figure 19(b)), 5400 seconds (Figure 19(c)), 7200 seconds (Figure 19(d)), and 10800 seconds (Figure 19(e)) of holding times, these

Systems	C_s (At. Pct)	Temperature range K (°C)	Source
B in Ni	0.3	1338.15 to 1383.15 (1065 to 1110)	[15,21–27]
B in Fe	0.1	1325.15 to 1523.15 (1052 to 1250)	[25,28–30]

times were not sufficient to achieve complete isothermal solidification. Even after 14400 seconds (Figure 19(f)), a joint free from secondary phases was not obtained. According to the experimental results, t_{IS} for the joints made using MBF-50 at 1448.15 K (1175 °C) was notably larger than that for the joints prepared using MBF-30 at 1333.15 K (1060 °C). It is worth noting that this is a significant departure from the expectation that an increase in bonding temperature should decrease the isothermal solidification time as predicted by the conventional TLP bonding model.

The average nominal residual liquid widths were plotted against the square root of holding time, as shown in Figure 20. The residual liquid widths in
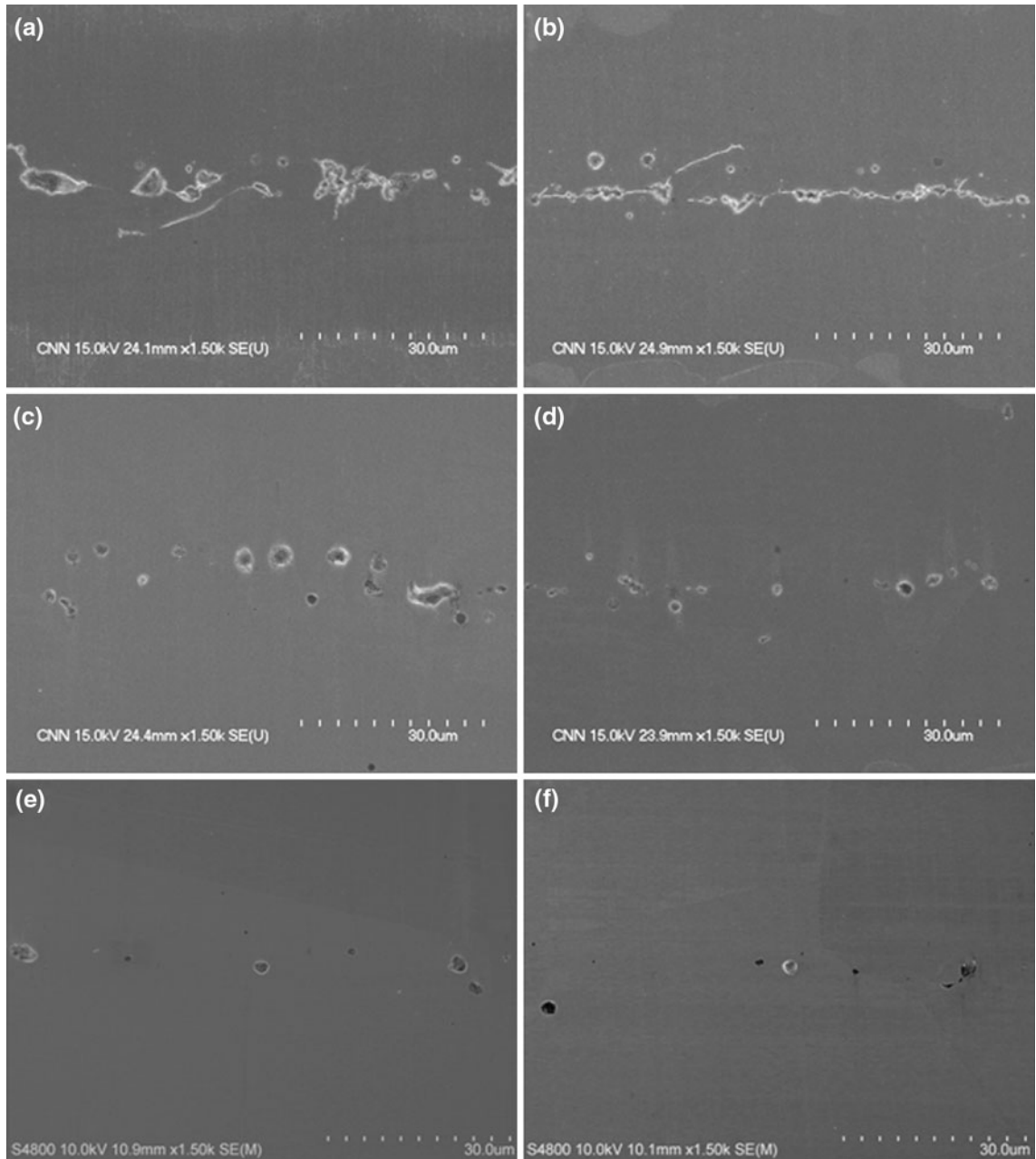

Fig. 19—SEM images of bonds prepared using MBF-50 at 1448.15 K (1175 °C) for 2700 s (*a*), 3600 s (*b*), 5400 s (*c*), 7200 s (*d*), 10800 s (*e*), and 14400 s (*f*).
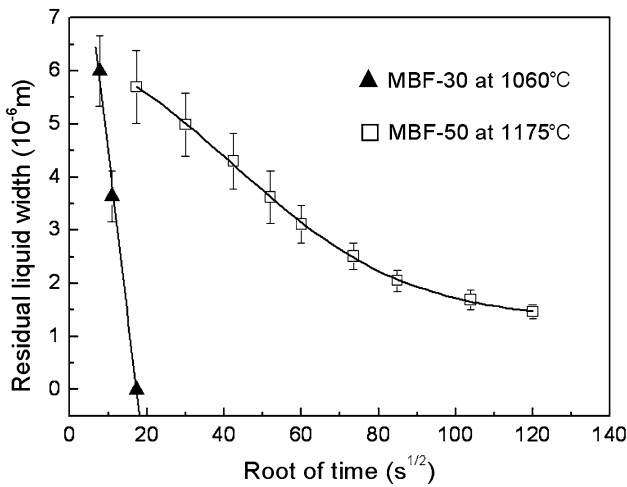
Fig. 20—Plot of residual liquid width against square root of holding time in joints using MBF-30 at 1333.15 K (1060 °C) and using MBF-50 at 1448.15 K (1175 °C).

MBF-30 joints decreased linearly with an increase in the square root of bonding time at 1333.15 K (1060 °C). In MBF-50, a considerable deviation from the linear relationship toward the end of the isothermal solidification took place. Also illustrated by the plot is a significant reduction in the rate of isothermal solidification with increased Cr and Si contents in the filler metal (from MBF-30 to MBF-50) and an elevated bonding temperature (from 1333.15 K to 1448.15 K [1060 °C to 1175 °C]).

E. Reduction in Isothermal Solidification Rate at Higher Temperature Using MBF-50 with a Lower B Content

Similar trends in other base and insert alloy systems in which an increase in bonding temperature above a certain temperature T_c, lead to the elongation of t_{IS} also have been observed.[19,24,38–42] An increased interdiffusion induced enrichment of base alloying elements, particularly Ti, in the liquated interlayer and a decrease in B solubility were suggested as plausible factors contributing to the deviation in isothermal solidification rate at higher bonding temperatures.[19,24,38–41]

It has been suggested by Sekerta[43] that an increase in bonding temperature might not necessarily lead to a faster solidification process, as the actual rate of solidification will depend on details of the phase relationships in complex alloy and on the diffusivities of solutes across the solid–liquid interface. Therefore, in multicomponent systems such as the present systems, DSS/MBF-30 and DSS/MBF-50, the observed phenomenon can be explained as follows:

(a) According to Fick's second law of diffusion, and assuming a constant diffusion coefficient the following is true:

$$\frac{\partial C}{\partial t} = D \frac{\partial^2 C}{\partial x^2} \qquad [6]$$

where $\partial C/\partial t$ is the change in solute concentration with time at a given position that can provide an

indication of the isothermal solidification rate, and $\partial^2 C/\partial x^2$ is the change in concentration gradient with distance. As mentioned, a reduction in the concentration gradient with distance between the interlayer and the substrate could be produced at 1448.15 K (1175 °C) using MBF-50. At any given instant, the concentration gradient ($\partial C/\partial x$) of a diffusing solute is decreased, and thus, $\partial^2 C/\partial x^2$ also is reduced. Obviously, Eq. [6] shows that the diffusion-controlled isothermal solidification rate is not only dominated by the diffusion coefficient but also by the concentration gradient, both of which could be influenced differently by bonding temperature. Interplay between the increase in diffusivity and the decrease in concentration gradient with an increase in temperature might be a factor contributing to the observed reduction in the isothermal solidification rate.

(b) Based on an analytical study of TLP bonding of binary systems, Tuah-Poku et al.[12] have developed the following equation to express the dependence of isothermal solidification completion time, t, on bonding temperature:

$$t = \frac{\pi W_0^2}{16 D_0} \left[\frac{\exp(Q/\mathrm{R}T)}{(C_{\alpha S})^2} \right] \qquad [7]$$

where W_0 is the initial liquid width and $C_{\alpha S}$ is the equilibrium solvus composition of the melting point depressant element. They qualitatively indicate that, as the temperature increases, t will reduce in terms of the exponential term. Nevertheless, an increase in bonding temperature simultaneously decreases the solvus composition (solid solubility),[33] $C_{\alpha S}$, and hence will tend to increase t. This suggests that time t may not continue to reduce monotonically with an increase in temperature but instead will tend to increase as the temperature reaches and exceeds a critical value in which the effect of reduced solubility overrides higher diffusivity.[19,24,38–42] It is plausible that the slower rate of isothermal solidification at 1448.15 K (1175 °C) is a consequence of the overriding influence of a decrease in B solubility relative to the increase in its diffusivity at this temperature.

(c) As stated in Section III–B, microstructural analyses reveal that the reduction in B diffusion from the interlayer resulted from the increase of Cr in the insert alloy. Thus, the substantial Cr might lead to an undesirable sluggish isothermal solidification rate.

(d) From previous work,[5] the commencement of a slower second solidification regime could be induced by an obvious increase in Si content. Thus, in the present study, a higher concentration of Si in MBF-50 may be a reason for the reduced isothermal solidification rate.

(e) It has been suggested that the formation of boride particles in the BAZ could remarkably increase the rate of isothermal solidification during the isothermal solidification stage.[44] Consumption of B by means of BN formation enables more B to

enter within the substrate, which has an accelerating influence on the effective B diffusion. Thus, this result can explain the overestimation *via* Eq. [4] at 1333.15 K (1060 °C) using MBF-30. However, at 1448.15 K (1175 °C), no BN precipitates were observed in the BAZ; hence, boride precipitation in this region has an inappreciable effect on the B diffusion when using MBF-50. Therefore, this finding also could be responsible for the decrease in the isothermal solidification rate at 1448.15 K (1175 °C).

IV. CONCLUSIONS

The following conclusions were drawn from this study:

1. Prior to the completion of isothermal solidification, Ni_3B and supersaturated γ-Ni formed in the ASZ and BN precipitates, which were observed in the BAZ of the specimen prepared with MBF-30 at 1333.15 K (1060 °C). However, BN and $(Cr, Ni)_3Si$ appeared in the ASZ, and the interface region was almost free of precipitates when using MBF-50 at 1448.15 K (1175 °C). This difference in the microstructure of the bond could result from the influences of Cr content, Si content, and bonding temperature.

2. Complete isothermal solidification, which avoided the formation of centerline eutectic constituent, occurred within 300 seconds at 1333.15 K (1060 °C) using MBF-30. Generally, a lower B content and a higher bonding temperature should lead to a smaller t_{IS}. However, a notable variance with the conventional expectation was observed in the joints made at 1448.15 K (1175 °C) using MBF-50. Even after holding for 14400 seconds, a joint with a precipitate-free centerline could not be obtained. It is suggested that the decreased isothermal solidification rate at 1448.15 K (1175 °C) using MBF-50 could be attributed to the following factors: (1) the decreased concentration gradient in B between the interlayer and the substrate, (2) the reduced B solubility, (3) the increased Cr content in the insert alloy, (4) the enhanced Si content in the filler material, and (5) the reduction of B flux into the base metal owing to lack of BN precipitates in the BAZ.

REFERENCES

1. T.I. Khan, N. Orhan, and M. Eroglu: *Mater. Sci. Technol.*, 2002, vol. 18, pp. 396–400.
2. L.H. Chiu, W.C. Hsieh, and C.H. Wu: *Mater. Sci. Eng.*, 2003, vol. 354A, pp. 82–91.
3. X.J. Yuan, C.Y. Kang, and M.B. Kim: *Mater. Charact.*, 2009, vol. 60, pp. 923–31.
4. X.J. Yuan, M.B. Kim, and C.Y. Kang: *Mater. Charact.*, 2009, vol. 60, pp. 1289–97.
5. X.J. Yuan, M.B. Kim, and C.Y. Kang: *Mater. Sci. Technol.*, in press.
6. S.D. Duvall, W.A. Owczarski, and D.F. Paulonis: *Weld. J.*, 1974, vol. 53, pp. 203–14.
7. G. Humpston and D.M. Jacobson: *Principles of Soldering and Brazing*, ASM International, Materials Park, OH, 1993, pp. 128–32.
8. O.A. Ojo, N.L. Richards, and M.C. Chaturvedi: *Sci. Technol.Weld. Join.*, 2004, vol. 9 (3), pp. 209–20.
9. C.Y. Su, C.P. Chou, W.J. Chang, and M.H. Liu: *J. Mater. Sci. Perform.*, 2000, vol. 9, pp. 663–68.
10. J.E. Ramirez and S. Liu: *Weld. J.*, 1992, vol. 71, pp. 365s–375s.
11. W.D. MacDonald and T.W. Eagar: *Metall. Mater. Trans. A*, 1998, vol. 29A, pp. 315–25.
12. I. Tuah-Poku, M. Dollar, and T.B. Massalski: *Metall. Trans. A*, 1988, vol. 19A, pp. 675–86.
13. Y. Zhou, W.F. Gale, and T.H. North: *Int. Mater. Rev.*, 1995, vol. 40 (5), pp. 181–96.
14. C.W. Sinclair, G.R. Purdy, and J.E. Morral: *Metall. Mater. Trans. A*, 2000, vol. 31A, pp. 1187–92.
15. O.A. Ojo, N.L. Richards, and M.C. Chaturvedi: *Sci. Technol. Weld. Join.*, 2004, vol. 9 (6), pp. 532–40.
16. W.F. Gale and E.R. Wallach: *Metall. Trans. A*, 1991, vol. 22A, pp. 2451–57.
17. D.M. Turriff and S.F. Corbin: *Metall. Mater. Trans. A*, 2008, vol. 39A, pp. 28–38.
18. M.L. Kuntz, S.F. Corbin, and Y. Zhou: *Acta Mater.*, 2005, vol. 53, pp. 3071–82.
19. M. Pouranvari, A. Ekrami, and A.H. Kokabi: *J. Alloys Compd.*, 2009, vol. 469, pp. 270–75.
20. The Japan Institute of Metals: *Metals Data Book*, The Japan Institute of Metals, Maruzen, Tokyo, 1993.
21. J.-D. Schöbel and H.H. Stadelmaier: *Z. Metallkde.*, 1965, vol. 56 (12), pp. 856–59.
22. T.B. Massalski: *Binary Alloy Phase Diagrams*, ASM, Metals Park, OH, 1986, pp. 366–71.
23. W.F. Gale and E.R. Wallach: *Mater. Sci. Technol.*, 1991, vol. 7, pp. 1143–48.
24. O.A. Idowu, N.L. Richards, and M.C. Chaturvedi: *Mater. Sci. Eng.*, 2005, vol. 397A, pp. 98–112.
25. M.A. Arafin, M. Medraj, D.P. Turner, and P. Bocher: *Mater. Chem. Phys.*, 2007, vol. 106, pp. 109–19.
26. K. Tokoro, N.P. Wikstrom, O.A. Ojo, and M.C. Chaturvedi: *Mater. Sci. Eng.*, 2008, vol. 477A, pp. 311–18.
27. M. Pouranvari, A. Ekrami, and A.H. Kokabi: *J. Alloys Compd.*, 2008, vol. 461, pp. 641–47.
28. *ASM Handbook: Alloy Phase Diagram*, vol. 3, ASM, Materials Park, OH, 1992, pp. 426–27.
29. B. Predel: *Physical Chemistry: Phase Equilibria Crystallographic Data and Values of Thermodynamic Properties of Binary Alloys*, Springer-Verlag, Heidelberg, Berlin, Germany, 1992, p. 15.
30. N.D. Luozzo, M. Fontana, and B. Arcondo: *J. Mater. Sci.*, 2007, vol. 42, pp. 4044–50.
31. E.A. Moelwyn-Hughes: *The Kinetics of Reaction in Solution*, Clarredon Press, Oxford, UK, 1947.
32. K. Nishimoto, K. Saida, D. Kim, and Y. Nakao: *ISIJ Int.*, 1995, vol. 35, pp. 1298–306.
33. J.E. Ramirez and S. Liu: *Weld. J.*, 1992, vol. 71, pp. 365s–375s.
34. A. Schnell: Ph.D. Thesis, Institut des Matériaux, Nantes, France, 2004.
35. A. Schnell and D. Graf: *Proc. 6th Int. Parsons Turbine Conf.*, 2003, pp. 971–85.
36. A. Sakamoto, C. Fujiwara, T. Hattori, and S. Sakai: *Weld. J.*, 1989, vol. 68, pp. 63–71.

37. J. Crank: *The Mathematics of Diffusion*, 2nd ed., Clarendon Press, Oxford, UK, 1975.
38. N.P. Wikstrom, O.A. Ojo, and M.C. Chaturvedi: *Mater. Sci. Eng.*, 2006, vol. 417A, pp. 299–306.
39. N.P. Wikstrom, A.T. Egbewande, and O.A. Ojo: *J. Alloys Compd.*, 2008, vol. 460, pp. 379–85.
40. A.T. Egbewande, C. Chukwukaeme, and O.A. Ojo: *Mater. Charact.*, 2008, vol. 59, pp. 1051–58.
41. M. Mosallaee, A. Ekrami, K. Ohsasa, and K. Matsuura: *Metall. Mater. Trans.*, 2008, vol. 39A, pp. 2389–2402.
42. O.A. Ojo and M.M. Abdelfatah: *Mater. Sci. Technol.*, 2008, vol. 24, pp. 739–43.
43. R.F. Sekerta: *Physical Metallurgy of Metals Joining*, TMS-AIME, St Louis, MO, 1980.
44. A. LeBlanc and R. Mevrel: *High Temperature Materials for Power Engineering Conference*, Liege, Belgium, 1990, pp. 1451–60.